X-ray emission after laser disintegration of clusters of carbon-containing molecules

E. S. Toma and H. G. Muller
FOM–Institute for Atomic and Molecular Physics, Kruislaan 407, 1098 SJ, Amsterdam, The Netherlands
(Received 8 March 2002; published 23 July 2002)

We present in this paper a study of the radiation emitted after the explosion of clusters of propane and carbon dioxide. The highly charged ions produced in the explosion can resonantly transfer an electron from the buffer gas, helium, into highly excited states. Radiation of wavelength as short as 11.6 nm was measured from O^{5+}, and shorter than 4 nm from C^{4+}.

DOI: 10.1103/PhysRevA.66.013205 PACS number(s): 36.40.−c, 32.30.−r

I. INTRODUCTION

In the attempt of obtaining radiation of very short wavelength, synchrotron facilities and hot plasmas emerged as the most popular sources of extreme ultraviolet (XUV) and soft x-ray radiation [1]. The synchrotron radiation is available in a wide range of wavelengths, and it is of high brightness. The disadvantages come from the duration of the pulses, in the picosecond range, and from the fact that large and expensive storage rings are necessary for the radiation production.

Hot and dense plasmas can easily be produced in the laboratory by focusing a high-power laser in a high-density target, or by capillary discharge. Such plasmas, of electron temperatures up to 1–2 keV, emit a weak continuum spectrum plus narrow lines from transitions in the present ions. In the case of laser-produced plasmas the time scale of the emission is in the picosecond range. For electrical-discharge plasmas, this time scale is longer, of the order 10 to few hundred nanoseconds. Coherent short-wavelength radiation of even subfemtosecond duration [2,3] can be obtained via high-harmonic generation [4]. Although easily available in the laser labs, the harmonic radiation is very weak, because of the very low conversion efficiency of the process.

Laser plasmas form also the lasing and amplification medium for XUV and soft x-ray lasers. The first x-ray laser was demonstrated at 21 nm by Matthews *et al.* in mideighties [5]. The plasma was formed by irradiation of a thin selenium foil with green light (532 nm) of 5×10^{13} W/cm^2 intensity in a linear focus, and the laser was pumped by electron-collisional excitation. Another experiment, based on recombination pumping via three-body collisions between one ion and two electrons, reported lasing at 18.2 nm in C^{5+} [6]. The three-body-recombination rate is proportionally dependent on n_e^3 and T_e^{-2}, thus high electron densities and low electron temperatures are necessary for achieving a high pumping rate that exceeds radiative recombination to other excited states. In Ref. [6] the plasma was created by a CO_2 laser in a solid carbon target and cooled by radiation losses. Since then, many experiments succeeded in proving (soft) x-ray lasing in plasmas [7].

Unfortunately, the plasma production in solid targets for x-ray lasers requires kilojoules of energy for the creation of highly charged ions, and the solid-density target is damaged and has to be renewed after each shot. In addition, the plasma blasted from the surface has steep density gradients. Using clusters as targets brings important improvements in this respect. The local density of the cluster is comparable to a solid target, and the target is renewed very simply in the jet flow. Like in a solid, collisional ionization in the expanding cluster helps the production of highly charged ions, and, using shorter laser pulses, much lower laser energies are sufficient [8]. After the clusters explode, a homogeneous plasma is formed very rapidly.

In a previous paper [9], we presented the measurement of ion production in Coulomb explosions of propane and carbon-dioxide clusters, describing also the mechanism of explosion. In this paper we go one step further and analyze the radiation emitted after the process of explosion. We focused our research on the process of resonant charge transfer as the main mechanism of excitation in the explosion-produced highly charged ions. This process is of high interest because recombination via charge transfer is faster than via three-body collisions.

The clusters are formed by adiabatic expansion from high pressure into the vacuum. The condensation is enhanced by mixing carbon-containing molecules (propane or carbon dioxide) with a light gas, helium. The laser is interacting with the cluster jet very close to the nozzle (Fig. 1), such that the clusters explode in an environment that contains a large density of helium atoms. Because it remains neutral in the laser field, the helium also acts as source of low-temperature elec-

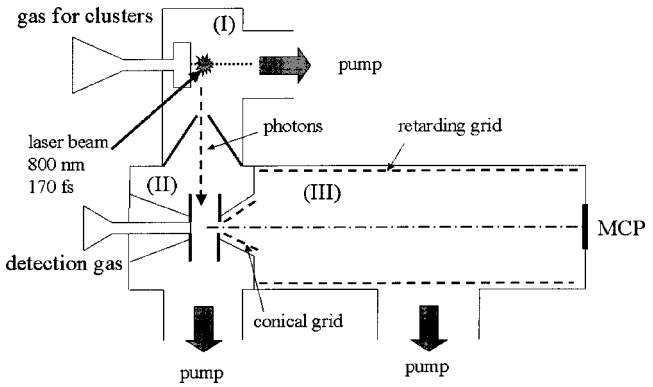

FIG. 1. Schematic of the experimental setup. (I) is the expansion chamber, where the clusters are formed. The jet flows horizontally and the infrared laser interacts with the clusters very close to the nozzle. The photons emitted by the highly charged ions produced in the explosion propagate into the spectrometer, interacting with the detection gas in chamber (II), and creating photoelectrons that are detected in the time-of-flight tube (III).

trons in the process of charge transfer. By collisions with the helium atoms, a highly charged ion can capture an electron into a highly excited state, from where the electron decays to the lower states, emitting photons. The charge-exchange process is resonantly enhanced if its initial and final state are degenerate.

The process of resonant charge transfer is described by the reaction:

$$A^{+z}+B\rightarrow A^{+z-1}+B^{+}.$$

This process is the prevailing one at impact velocities lower than 10^3 km/s. At higher velocities, impact ionization becomes dominant. The total cross sections are reasonably large, 10^3 Mb for C^{3+} and 2.5×10^3Mb for C^{5+} colliding with H at 50 keV [10]. The contribution is mostly due to resonant charge transfer to excited states that at some interaction distance cross the energy level of the electron on the source atom. The cross section for O^{6+} in collision with He, in the $n=3$ levels of O^{5+}, bound at $\simeq -55$ eV is 7×10^{-16} cm^2, while in the $n=4$ levels, bound 25 eV higher, it is less than 10^{-16} cm^2 (at 10 eV) [11].

In our experiment the neutral is helium, of ionization potential $I_p=24.6$ eV, so only states of binding energy lower than this I_p are likely to capture electrons. There are also carbon neutrals in the outer fringes of the focus, where the intensity is lower than 3×10^{13} W/cm^2, but, with an average path of $\simeq 5$ μm, the ions formed in the most intense part of the focus are not likely to escape to those regions without being partly neutralized. On the other hand, for the experiment on propane (C_3H_8), neutral H resulting from dissociation of H_2^+ can also transfer electrons, but the amount of H_2^+ is far less than helium. We cannot exclude the case that some ions are excited by collisions with fast electrons in the explosion process, but numerical simulations suggest that the probability of such an event is very low [9].

In our setup, we detect the photons in an indirect way, through electron spectroscopy. The photon spectrum is reconstructed by measuring the energy spectrum of electrons created by these photons in the ionization process of a detection gas.

II. EXPERIMENTAL SETUP

The experimental setup is similar to that described in Ref. [9], and can be seen in Fig. 1. The cluster explosion is done in a chamber installed on the top of a magnetic-bottle electron spectrometer. The jet containing the clusters flows horizontally through this chamber and is crossed by the laser at a distance of 5 mm from the pulsed valve. Highly charged ions, hot electrons, and photons are produced in the process of cluster explosion. The explosion chamber is separated by a 1.5aperture from the ionization chamber, which acts as a gas resistance for differential pumping. The radiation emitted in the explosion propagates in a straight line to the ionization chamber, where it ionizes the atoms of the detection gas. A strong magnetic field applied between the pole pieces collects half of the photoelectrons and guides them towards the time-of-flight (TOF) tube, where the electron trajectories are parallelized by the adiabatic transition to a weak magnetic field. The electrons are detected after 1 m by microchannel plates.

The energy resolution of the spectrometer is $\simeq 5\%$. A retarding voltage could be applied on a cylindrical grid, inside the flight tube, slowing down the electrons. Because of imperfect parallelization of the trajectories of the high-energy electrons, cyclotron oscillations spaced by 80 ns can appear and can be detected in the spectrum close to the retarding-voltage edge, where the resolution is high enough. The overall detection efficiency of the spectrometer is roughly 25%.

In the adiabatic expansion, the mixture of propane and helium or CO_2 and helium cools to the saturation point after which the molecules condensate into clusters. The light atomic gas, helium, enhances the cooling by increasing the adiabatic constant of the mixture, favoring the formation of clusters from gases that would not condense in pure form (the case of propane). The nozzle had a diameter $d=500$ μm and an angle of 45°. From the theory of expansion [12], we estimated that at 5 mm from the nozzle, the temperature dropped to $0.05T_0$, (where T_0 is the source temperature), and the particles reached already the terminal velocity $v_\infty=\sqrt{2c_pT_0}(=1.3$ km/s for a 15% mixture of propane and He, and slightly less for the mixture containing CO_2), where c_p is the specific heat of the mixture. The density changes in the expansion according to

$$n=n_0\left(\frac{T}{T_0}\right)^{1/(\gamma-1)}=n_0\left(1+\frac{\gamma-1}{2}M^2\right)^{-1/(\gamma-1)},$$

where γ is the adiabatic constant of the mixture (1.4 for 15% propane and 1.56 for 15% CO_2), and M is the Mach number, given by the ratio v/a, a being the local speed of sound. The location of the Mach disk, where the shock transition to a subsonic flow occurs, is quite insensitive to γ and is given by $(x_M/d)=0.67(p_0/p_b)^{1/2}$. For a backing pressure $p_0=20$ atm and a background pressure $p_b=10^{-10}$ atm, which we usually had in the experiment, the terminal Mach number (31 for propane) is reached after 150 m. Of course, our setup was much shorter, and the shock waves were of no concern. At 5 mm from the nozzle, the density is $\simeq 3\times10^{17}$ cm^{-3}, 1000 times lower than at the source, and the collision frequency drops 10000 times [12]. We conclude that by this distance, the clusters are already formed and follow a collision-free flow.

III. RESULTS

When measuring the electron TOF trace, a very strong signal was detected at more than 1 μs, which did not move or disappear when changing the retarding voltage. This signal was caused by secondary electrons produced in the collisions of the photoelectrons with the walls of the right-hand-side pole piece. These secondaries had energies lower than 5 eV and were created in a region of high potential, thus unretardable by the cylindrical grid. The conical grid inside the pole piece was therefore disconnected from the grid in the flight tube, so that it could be connected to a voltage 5 V less

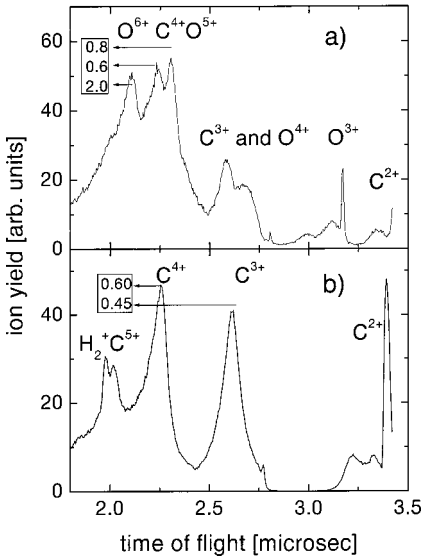

FIG. 2. (a) Ion spectrum from Coulomb explosions of CO_2 clusters of $\simeq$4500 molecules, at a laser intensity of 3.5×10^4 W/cm^2. (b) Ion spectrum from Coulomb explosions of propane clusters of $\simeq$50 000 molecules, at the same laser intensity. The two little insets show, in keV, the kinetic energies of the most important ions at the peak position. The very narrow peaks correspond to ions created by direct optical-field-induced ionization of isolated molecules.

negative than this main grid. This eliminated the secondary electrons from the spectrum, while still retarding the electrons as early as possible in the parallelization process.

Free electrons produced in the cluster explosions cannot pass through the strong magnetic field applied on the two conical pole pieces, and thus do not give any contribution to the detected signal. Two vertical plates were installed below the skimmer to deflect ions from a possible trajectory from explosion chamber towards the ionization point. This, however, caused no change in the observed signal. We can safely say that the electrons detected in the TOF tube come exclusively from photoionization of the detection gas.

A. CO_2

In the first experiment, we irradiated clusters of CO_2 of 3500 molecules on average. This cluster size was determined with a relative error of 50%, using the Rayleigh-scattering technique [9,13]. Although taken at a lower pressure, the ion spectrum is very similar to that in Fig. 2(a), obtained from somewhat larger clusters. The highest charge states observed were O^{6+} and C^{4+}. The C^{5+} ions should have appeared at 2.2 μs if produced with zero initial kinetic energy. This time region is covered by the tail of O^{6+} peak. The difference in ionization potential between O^{6+} and C^{5+} is 254 eV, and we tend to believe that no significant amount of C^{5+} was produced.

Note that for the spectra in Figs. 2(a) and 2(b), the cluster disintegration took place 20 cm from the nozzle, compared to a distance of only 5 mm now. We also used a more intense beam, 10^{15} W/cm^2 for the present experiment, focused slightly behind the gas jet in order to increase the focal volume, so that the clusters were exposed to an intensity of 3×10^{14} W/cm^2. For the radiation spectra, the volume increase made an important difference in terms of number of counts. Except for these differences, we maintained all the other parameters, of the gas source and of the laser, the same.

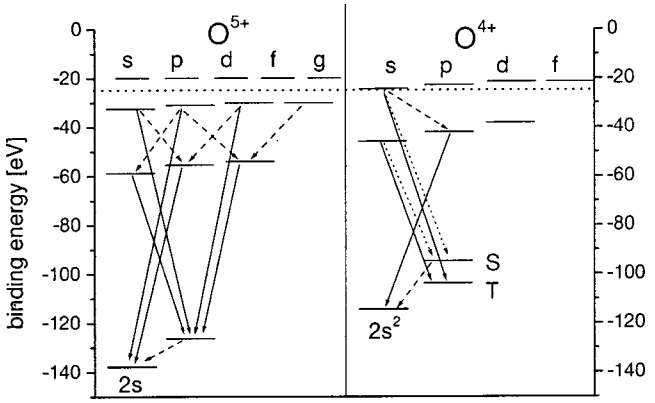

FIG. 3. Level schemes in O^{4+} and O^{5+}. The solid arrows indicate observed transitions, while the dashed arrows indicate transitions of too low an energy to be detected by photoionization of neon (also because of the secondary electrons), but which are expected to occur. The dotted arrows in O^{4+} represent singlet transitions that do not appear clearly in the spectrum. The singlets and the triplets for states of $n\geqslant3$ in O^{4+} are too close to be depicted separately. The dotted horizontal line near the top of the figure marks the binding energy of the ground state of helium.

We used helium and neon as detection gases of the emitted radiation. Helium has the advantage of a simpler atomic structure, making it possible to unambiguously deduce the photon energy from the observed energy of the photoelectron. In the case of neon ($1s^22s^22p^6$), ionization can take place from both the $2p$ and the $2s$ level if the photon energy exceeds 48 eV. Nevertheless, the absorption cross section of Ne is larger than that of He (σ_{Ne} changes between 9 and 3 Mb in the region 21.6–124 eV; $\sigma_{\mathrm{He}}=0.3$–7 Mb for the same region, with values lower than 1 Mb for more than 62 eV [14]). We were especially interested in the region 90 to 120 eV (10.3–13.8 nm), where the most energetic transitions occurred in O^{5+} (Li-like ion, with an ionization potential of 138 eV), from the $n=4$ levels to the L shell (see Fig. 3). Assuming C^{4+} to be the highest ionic state of carbon resulting from the explosion, the charge transfer can produce then excited C^{3+}, also Li-like, but with $I_p=64.5$ eV, from which we did not expect transitions of more than 40 eV.

The quality of the helium spectra is quite poor because of the low counting rate, but these spectra help us to distinguish between the lines due to $2p$ ionization and the lines due to $2s$ ionization in neon. We present in Fig. 4 photoelectron spectra of neon measured at different retarding voltages. The contribution of carbon consists of only three lines, all in C^{3+}: $3s,d\rightarrow2p$ at 29.6 and 32.3 eV (peak 1), and $3p\rightarrow2s$ at 40 eV (peak 2). The M-shell states in C^{3+} have binding energies of -27–-24 eV ([15] for all energy levels in this paper). All the transitions involved in the following discussion are presented in Table I.

Oxygen accounts for most of the lines in the spectra, with transitions in three ionic states. The M shell in O^{3+} has states

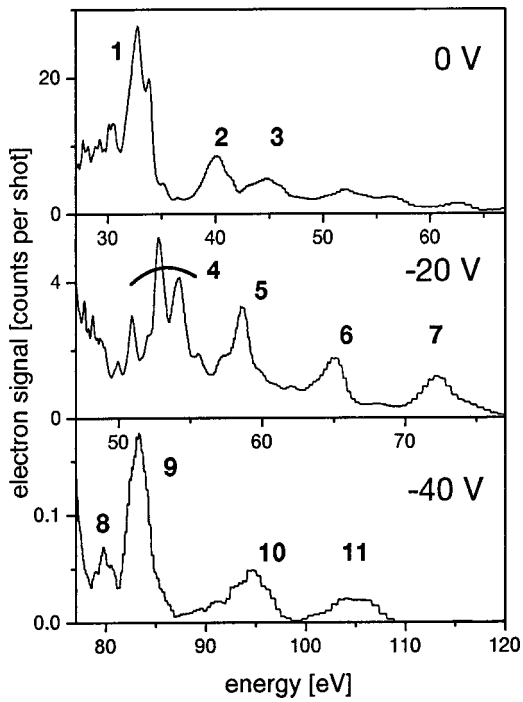

FIG. 4. Neon spectra produced by ionization with photons emitted in the explosion of 3500-molecules CO_2 clusters, at different retarding voltages: 0, -20, and -40 V, from top to bottom. The ionization potential of neon (21.6 eV) was added to the detected kinetic energies of the electrons, and to the retarding potential in the energy scale.

of $n=3$ bound between -25 and -33 eV, and probably all of them are populated via charge transfer but only the two transitions to $2p$ occur, at 44.3 and 52 eV (peaks 3 and 4), because the $2s$ level is already occupied. The substructures of peak 4 is probably not real, but an artifact of the spectrometer, for reasons explained in the section describing the setup.

In O^{4+}, with the exception of $4s$, all levels of the N shell are bound above -24 eV, and do not capture electrons by charge transfer. Excited states of O^{4+} already have one electron in the $2s$ ground state, whose interaction with the excited electron splits the excited states into singlets and triplets. (If the spacing between the triplet and the singlet state is small, the state is depicted as only one line in Fig. 3.) The level $4s$ decays to $3p$ (17.6 eV for the triplet, and 18.6 eV for the singlet transition) or to $2p$ emitting a photon of 79.4 eV (peak 8) in the triplet transition, or 71 eV in the singlet transition, which does not appear clearly in the spectrum. The transition $2s4p \rightarrow 2s^2$ at 91.5 eV (13.6 nm) was not detected. The singlet transition $2s3p \rightarrow 2s^2$, at 72.3 eV, is visible in peak 7. From the four transitions $3 \rightarrow 2p$, only the triplet $3s \rightarrow 2p$ at 57.6 eV appears as peak 5 in Fig. 4. If the singlet $3s \rightarrow 2p$ at 50 eV might be hidden in the structure of peak 4, there is no trace of the two $3d \rightarrow 2p$ transitions at 56.3 and 64.3 eV.

The lines of O^{5+} are the most important. The K shell of O^{5+} is completely filled and the ground state is thus $2s$. The levels of $n=5$ are lying above the ionization potential of He, somewhere at -20 eV, and most probably are not populated (Fig. 3). The transition $5p \rightarrow 2s$ at 118 eV (10.5 nm) was not observed. The capture can occur on the levels of $n=4$, bound in the range -32.4–-30.6 eV. The transitions $4 \rightarrow 3$ have quite low energies, 23–28 eV, making them of less practical interest, but in the transitions $4 \rightarrow 2$ photons of very short wavelength are emitted. The probability to go from $n=4$ to $n=2$ is higher then from 4 to 3, excepting $4f$, of course (60% for $4s$, 77% for $4p$ and d). The transition $4s \rightarrow 2p$ at 94 eV (13.2 nm), contributes to peak 10 together with $4d \rightarrow 2p$ at 95.5 eV (13 nm). Peak 11 is the result of transition $4p \rightarrow 2s$ at 107 eV (11.6 nm). The three transitions $3 \rightarrow 2$ are also visible in the spectrum: $3p \rightarrow 2s$ as peak 9 (82.6 eV), $3s \rightarrow 2p$ as peak 6 (67.4 eV), and $3d \rightarrow 2p$ in peak 7 (71.7 eV).

The number of photoelectrons detected in our setup (N_e) is related to the number of photons that were originally produced in the cluster explosion and subsequent charge transfer (N_{photons}) by a proportionality factor that involves the gas pressures in both jets, photoionization cross sections, and

TABLE I. Table of transitions.

Ion	Transition	Energy (eV)	In CO_2 (Fig. 4)	In C_3H_8 (Fig. 6 Ar)
O^{3+}	$3d$-$2p$	52	4	
	$3s$-$2p$	44.3	3	
	$4s$-$2p(S)$	71		
	$4s$-$2p(T)$	79.4	8	
	$3d$-$2p(S)$	56.3		
O^{4+}	$3d$-$2p(T)$	64.3		
	$2s3p$-$2s^2$	72.3	7	
	$3s$-$2p(S)$	50	4	
	$3s$-$2p(T)$	57.6	5	
	$4d$-$2p$	95.5	10	
	$4p$-$2s$	107	11	
O^{5+}	$4s$-$2p$	94	10	
	$3d$-$2p$	71.7	7	
	$3p$-$2s$	82.6	9	
	$3s$-$2p$	67.4	6	
	$3d$-$2p(S)$	21.6		1
	$3d$-$2p(T)$	27		2
C^{2+}	$2s3p$-$2s^2$	32.1		4
	$3s$-$2p(S)$	18		
	$3s$-$2p(T)$	23		1
	$3d$-$2p$	32.3	1	4
C^{3+}	$3p$-$2s$	40	2	6
	$3s$-$2p$	29.6	1	3
	$3d$-$2p(S)$	47.3		7
	$3d$-$2p(T)$	50		7
	$3p$-$2s(S)$	51.6		8
C^{4+}	$3p$-$2s(T)$	54.6		8
	$1s3p$-$1s^2$	354.4		Auger
	$3s$-$2p(S)$	45.3		7
	$3s$-$2p(T)$	47.5		7
	$1s2p$-$1s^2$	308		Auger

geometric factors. The number of counts we have is $N_e = (N_{\text{photons}}/S) c_{\text{eff}} N_{\text{at}} \sigma_{\text{ionz}}$, where $S = 4\pi r^2$ ($r = 20$ cm being the distance from the source to the detector axis), c_{eff} is the detector efficiency ($\simeq 25\%$), N_{at} the number of atoms exposed in the sensitivity volume of the spectrometer, and σ_{ionz} the ionization cross section of the detection gas. Even if the estimation of the detection gas density between the pole pieces cannot not be done with much accuracy, it is still useful to give even a rough value for the number of photons produced after the explosion. The contribution of carbon via low-energy lines in C^{3+} (peaks 1 and 2) amounts to 2×10^{11} photons, which is equal to the contribution of O^{3+}, O^{4+}, and O^{5+} together. The number of photons of 11.6 nm (peak 11) is $\simeq 0.8 \times 10^9$, and the number of photons in peak 10, from two transitions, is $\simeq 10^9$, according to our calculations. These values are corrected for the angular selectivity of the detection scheme, assuming isotropic emission, and they represent numbers of photons in the focus.

The ionization threshold for the $2s$ level in neon is $\simeq 47.6$ eV, so each peak in the spectra shall have a companion at an energy lower by $\simeq 26$ eV. For different reasons, these additional transitions do not appear clearly in the spectrum. Peaks 11, 10, 9, and 8, are small themselves, and their companions (approximately at 81, 69, 57, and 53 eV) are hidden by other peaks or in the background. The companions of peaks 7, 6, and 5 (at 46, 41, and 32 eV) coincide accidentally with peaks 3, 2, and 1, respectively, and mix with other transitions.

B. C_3H_8: Auger decay in argon

The large propane clusters, 50 000 molecules on average, allowed the production of C^{5+} [Fig. 2(b)]. The detection of radiation was done with helium and argon. Because of the larger number of molecules in the cluster, the radiation emission increases, and the quality of the helium spectrum is pretty good, although not much is measured beyond 65 eV due to the rapid decrease of the helium cross section. Argon has a very high ionization cross section, $\simeq 12$ Mb from 15.8 eV, the ionization potential by removing a $3p$ valence electron, to 29 eV, which is the threshold for $3s$ ionization. After this range the cross section drastically drops to $\simeq 0.2$ Mb, only to increase to 4 Mb at 248 eV, the edge of L-shell ionization [14]. It is this L-shell edge that makes argon very useful for our measurement, because it permits the detection of high-energy transitions (more than 300 eV) to the K shell in C^{4+} (or eventually C^{5+}) via an Auger-decay process in argon.

An Auger process consists of photoionization from an inner shell, followed by the decay of an electron from a higher level to fill the hole, the excess energy being released in the excitation or ionization of another high-level electron. Thus two free electrons result from this process: the primary electron, which has an energy equal to the energy of the photon minus the inner-shell edge, and the Auger electron (if released into the continuum) of energy equal to the energy gained in the Auger decay minus its binding energy. The configuration of Ar is $1s^2 2s^2 2p^6 3s^2 3p^6$. L-shell photoionization can occur by removing an $s(L_1)$ or a p electron (L_{23})

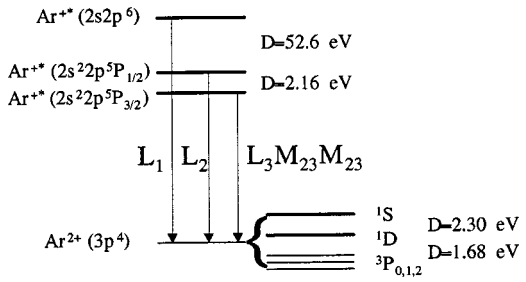

FIG. 5. Level scheme of $Ar^{+}*$ and Ar^{2+} including only the states that intervene in the Auger process described in this chapter.

by a photon of more than 313 or 248 eV, respectively. The state of configuration $2p^5 3s^2 3p^6$ in $Ar^{+}*$ is a doublet spaced by 2.16 eV (Fig. 5). The ground state of configuration $2p^6 3s^2 3p^4$ in Ar^{++} is split by the spin-orbit interaction in state $^1S_0, ^1D_2$, and the triplet $^3P_{0,1,2}$. Thus ten transitions of type $L_{23}M_{23}M_{23}$ can occur at energies between 201 and 207.14 eV, and five of type $L_1 M_{23} M_{23}$ in the range 279–283 eV [16–18].

In Fig. 6 we present two spectra taken on Ar and He, at 0-V retarding voltage. The signal drops significantly in the Ar spectrum above 35 eV, but the main differences are the absence of peak 5 in the Ar spectrum (peak 7 can be seen on a smaller scale), and the different ratio between peaks 3 and 4 in the two spectra (although peak 3 is raised on the slope of the secondary electrons in the He spectrum). Ar spectra (or He) taken on different days showed to be quite similar to each other. More to it, we could not assign any carbon transition to peak 5. The $5 \rightarrow 3$ transition in C^{5+} occurs indeed at 35 eV, but the amount of C^{6+} we create (if at all) is certainly too little to explain such a strong line.

Peaks 1 and 2 are lines in the doubly charged carbon: the $3d \rightarrow 2p$ transitions at 21.6 eV (singlet) and 27 eV (triplet), and the triplet $3s \rightarrow 2p$ transition at 23 eV (the singlet occurs at 18 eV and cannot be seen because of the secondary electrons). The singlet $2s3p \rightarrow 2s^2$ at 32.1 eV contributes to peak 4 (see also Table I). The M-shell states in C^{2+} have binding energies between -13.6 and -15.8 eV. Population of these

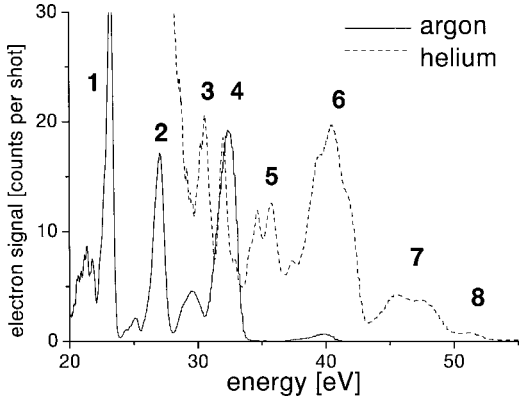

FIG. 6. Argon (solid line) and helium (dashed line) spectra produced by ionization with photons emitted in the explosion of 50 000-molecules C_3H_8 clusters, measured without retarding voltage. The spectra are scaled including the ionization potential of the detection gas.

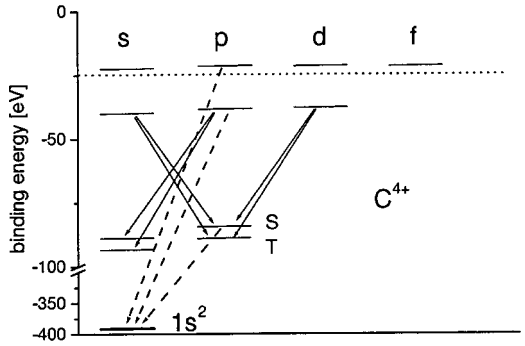

FIG. 7. Level scheme in C^{4+}. The solid arrows indicate transitions detected directly, while the dashed arrows indicate transitions observed via an Auger-decay process in argon. The singlets and the triplets for states of $n \geqslant 3$ are not depicted separately. The dotted horizontal line near the top of the figure marks the binding energy of the ground state of helium. The vertical scale is broken between -100 and -300 eV.

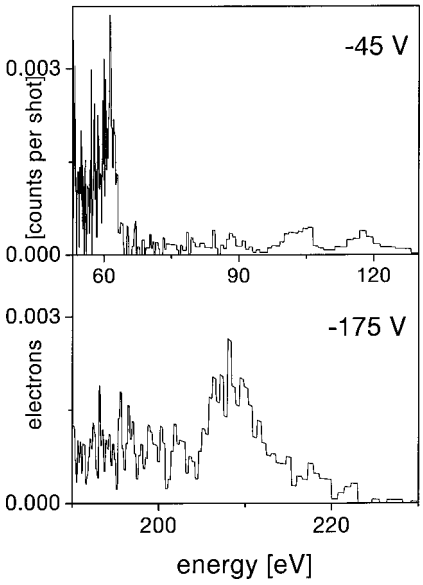

FIG. 8. Argon spectra at two different retarding voltages: -45 and -175 eV. The ionization potential of argon is not included in the energy scales.

levels from helium should thus be energetically impossible, which makes appearance of these lines rather puzzling. The possibility exists that they are populated by charge transfer from hydrogen atoms produced by cluster explosions in the lower-intensity regions of the focus. Transitions in triply charged carbon appear in peaks 3, 4, and 6: $3s,d \rightarrow 2p$ at 29.6 and 32.3 eV, $3p \rightarrow 2s$ at 40 eV. The wide peak 7 and the small peak 8 result from $3 \rightarrow 2$ transitions in C^{4+} (Fig. 7). There are three triplet transitions and three singlet transitions, four at energies between 45.3 and 50 eV, with $2p$ as final state, and two at 51.6 and 54.6 eV with final state $2s$.

There is no signal detected in the He spectrum after 55 eV, which suggests that there are no transitions to $n=2$ from $n=4,5\ldots$ in C^{4+} (or $n=3,4\ldots$ in C^{5+}). Nevertheless, with Ar as detection gas, there are electrons present in the spectrum at very high energies, in the range 203–215 eV [Fig. 8(b)], which is the energy range of Auger electrons from $L_{23}M_{23}M_{23}$ transitions. (The $L_1M_{23}M_{23}$ transitions could not be clearly detected.) The low counting rate and the poor resolution make any attempt to distinguish individual lines futile. The peak in Fig. 8(b) sums all Auger electrons. Only transitions to the ground state in C^{4+} (or C^{5+}) have energies larger than 248 eV, and they are responsible for the production of these electrons. From the low-energy spectrum we know that states of principal quantum numbers 3 or 2 are certainly populated, so we focus our attention on transitions from the singlet states $3p$ and $2p$ to the ground state. To make the identification we have to look for the primary electrons, as well. If the 308-eV (4-nm) photon emitted in the $1s2p \rightarrow 1s^2$ transition of C^{4+} L-shell ionizes Ar, an electron of 60 eV is created, while an electron of 106.4 eV is produced by the 354.4-eV (3.5-nm) photon of the deexcitation $1s3p \rightarrow 1s^2$. These electrons do appear in Fig. 8(a) as the first two peaks in the spectrum. (The energy scales of Fig. 8 do not include the ionization potential of Ar, they only indicate detection energies plus the retarding potential.) There is also a third peak in Fig. 8(a), at $\simeq 118$ eV, which is most likely produced by L-shell photoionization of Ar with a 371-eV (3.3-nm) photon from the transition $1s4p \rightarrow 1s^2$, although we do not have any clear evidence from the low-energy part of the spectrum that the levels of $n=4$ are populated. The $1s3p,4p \rightarrow 1s^2$ transitions have very small branching ratios: 0.03 and 0.01, respectively. The main contribution to the Auger peak belongs to photons emitted in the $1s2p \rightarrow 1s^2$ transition.

The estimated total number of photons triggering the Auger decay is 0.54×10^9, in accordance with the number given by the peaks of primary electrons. The contribution of the 4-nm photons is 67% of it, the other two lines share equally the rest.

IV. CONCLUSIONS

From the large number of photons with energy more than 248 eV (0.54×10^9), for example, we detect only 0.015 per shot, due to our very low detection efficiency, $\simeq 3 \times 10^{-11}$. At 30 eV, also on argon, the detection efficiency is only three times larger. One (negative) conclusion of this experiment is the fact that electron spectroscopy is not an efficient method of detecting radiation, unless the detection could occur very close to the source, where the density of photons is larger.

On the other hand, it is encouraging that so many photons are produced, and that the charge-transfer process occurs with such a high probability. The total number of photons indicated by the argon spectrum is $\simeq 10^{12}$, while we estimate the numbers of carbon atoms in the focus to be $\simeq 3.5 \times 10^{12}$. If 80% of the propane molecules are forming clusters, this means 2.8×10^{12} potential emitters. C^+ and C^{2+} cannot transfer electrons from helium because of their low electron affinities, but they make only 10% of the ions. C^{5+} ions are actually able to transfer electrons three times till they reach the C^{2+} state, and C^{4+} twice. The number of potential emitters is thus 4.6×10^{12}, which gives 22% for the transfer efficiency. Since this value is based on estimates of pressures in various gas jets, it contains large uncertainties

and should be viewed more as an indication of the order of magnitude.

We cannot estimate what subshells are preferentially populated, because we cannot always resolve individual lines. Nevertheless, our data confirm the fact that O^{5+} captures electrons mainly in the *M* shell (around 10 to 15 times more than in the *N* shell, including the correction for $4 \rightarrow 3$ deexcitations). All other ions capture electrons only in the *M* shell, the first energetically allowed to transfer electrons from helium, except for O^{4+}, which also gets electrons in level $4s$.

A rough estimate of the energy balance of the propane cluster explosion is as follows. The 2.8×10^{12} carbon ions carry an average kinetic energy of $\simeq 400$ eV per particle (as the results of Ref. [9] indicate), which makes a total of 1.1×10^{15} eV. Most of the hydrogen ions have very small kinetic energies, and we will neglect them. The energy needed to create the ions is, according to the charge-state percentages indicated by Fig. 2(b), $\simeq 0.5 \times 10^{15}$ eV. We estimated the number of electrons at $\simeq 10^{13}$, and using for the average kinetic energy per electron the value given by the numerical calculations described in Ref. [9] ($\simeq 50$ eV, at the end of the pulse), we find a total of 0.5×10^{15} eV. We seem to produce $\simeq 10^{12}$ photons of more than 16 eV. The average energy per photon is roughly 100 eV, which amounts to 0.1×10^{15} eV. We can conclude that only a small fraction (5.5%) of the total energy of the 6-mJ pulse used in the experiment is actually absorbed by the clusters, which is consistent with our experimental observations. 23% is used for ionization, 50% of the absorbed energy is converted into ionic kinetic energy, 23% is taken by the electrons, and only 4% is converted into photons.

ACKNOWLEDGMENTS

This work is part of the research program of FOM (Fundamental Research on Matter), which is subsidized by NWO (Netherlands Organization for the Advancement of Research).

[1] D. Attwood, *Soft X-Rays and Extreme Ultraviolet Radiation* (Cambridge University, New York, 2000).
[2] P. M. Paul *et al.*, Science **292**, 1689 (2001).
[3] M. Hentschel *et al.*, Nature (London) **414**, 509 (2001).
[4] P. Saliéres, A. L'Huillier, P. Antoine, M. Lewenstein, Adv. At., Mol., Opt. Phys. **41**, 83 (1999).
[5] D. L. Matthews *et al.*, Phys. Rev. Lett. **54**, 110 (1985).
[6] S. Suckewer, C. H. Skinner, H. Milchberg, C. Keane, and D. Voorhees, Phys. Rev. Lett. **55**, 1753 (1985).
[7] R. C. Elton, *X-Ray Lasers* (Academic, San Diego, 1990).
[8] T. Ditmire, T. Donnelly, A. M. Rubenchik, R. W. Falcone, and M. D. Perry, Phys. Rev. A **53**, 3379 (1996).
[9] E. S. Toma and H. G. Muller, Phys. Rev. A **66**, 013204 (2002).
[10] R. E. Olson and A. Salop, Phys. Rev. A **77**, 531 (1977).
[11] J. P. M. Beijers, R. Hoekstra, A. R. Schlatmann, R. Morgenstern, and F. J. de Heer, J. Phys. B **25**, 463 (1992).
[12] D. R. Miller, in *Atomic and Molecular Beam Methods*, edited by G. Scoles (Oxford University, New York, 1988), Vol. I, p. 14.
[13] T. Ditmire *et al.*, Phys. Rev. A **57**, 369 (1998).
[14] J. Berkowitz, *Photoabsorption, Photoionization, and Photoelectron Spectroscopy* (Academic, New York, 1979).
[15] C. E. Moore, *Atomic Energy Levels*, Nat. Bur. Stand. (U.S.) Circ. No. 467 (U. S. GPO, Washington, D.C., 1949).
[16] K. G. Dyall and F. P. Larkins, J. Phys. B **15**, 2793 (1982).
[17] J. Bruneau, J. Phys. B **16**, 4135 (1983).
[18] J. M. Schins *et al.*, Phys. Rev. A **52**, 1272 (1995).